Charge transport, injection, and photovoltaic phenomena in oligo(phenylenevinylene) based diodes

Melzer, Christian; Krasnikov, Victor V.; Hadziioannou, Georges

Published in:
Journal of Polymer Science. Part B: Polymer Physics

DOI:
10.1002/polb.10639

Publication date:
2003

Charge Transport, Injection, and Photovoltaic Phenomena in Oligo(phenylenevinylene) Based Diodes

CHRISTIAN MELZER, VICTOR V. KRASNIKOV, GEORGES HADZIIOANNOU*

Department of Polymer Chemistry, Material Science Center, University of Groningen, Nijenborgh 4, 9747 AG Groningen, The Netherlands

Received 31 January 2003; revised 14 March 2003; accepted 14 March 2003

ABSTRACT: We report on the charge transport and injection phenomena of (*E*,*E*,*E*,*E*)-1,4-bis[(4-styryl)styryl]-2-methoxy-5-(2′-ethylhexoxy)benzene (MEH-OPV5) sandwiched between asymmetric contacts. The hole mobility of MEH-OPV5 was determined by means of transient electroluminescence. The steady-state current was injection-limited. The electric field and temperature dependence of the current were quantitatively described by a phenomenological injection model of thermally assisted charge-carrier tunneling in a one-dimensional chain of hopping sites. Furthermore, we report on the photovoltaic properties of thin-film photovoltaic cells on the basis of donor–acceptor heterojunctions. MEH-OPV5 and buckminster fullerene were used as the donor and acceptor materials, respectively. The emphasis was on the role of morphology in such devices. © 2003 Wiley Periodicals, Inc. J Polym Sci Part B: Polym Phys 41: 2665–2673, 2003

Keywords: charge transport; photophysics; interface; morphology

INTRODUCTION

In the last decade, the potential of organic materials in the field of electronics, such as active semiconductors, triggered novel interest in material sciences, chemistry, and physics. Although organic light-emitting diodes are already commercially available, the efficiencies of organic solar cells[1–5] are still lower than those of their inorganic counterparts.[6] This demands an intensive search for more efficient organic materials for photovoltaics and a better understanding of the device physics.

The photovoltaic effect involves the creation of free electrons and holes under optical excitation and their successive collection at opposite electrodes. In organic semiconductors, illumination creates mainly excitons that need to dissociate into free holes and electrons that are collected at the electrodes. Exciton dissociation occurs rather efficiently at the interface of two materials with different ionization potentials and electron affinities, which lead to the inception of donor–acceptor-like photovoltaic systems.[1,2,7]

Although many studies have been carried out, charge-transport and injection phenomena occurring in devices of organic semiconductors are still not sufficiently understood but are nonetheless of major importance for the device operation. Because of the hopping nature of transport and apparent energy and positional disorder, transport models developed for inorganic semiconductors[8] fail to describe the experimental observations. Here we report on charge transport through single-layer cells on the basis of the donor (*E*,*E*,*E*,*E*)-1,4-bis[(4-styryl)styryl]-2-methoxy-5-(2′-ethyl-

**Present address:* Ecole Européenne Chimie Polymères Matériaux (ECPM), Université Louis Pasteur Strasbourg, 25, rue Becquerel, F-67087 Strasbourg Cedex 2, France

Correspondence to: V. V. Krasnikov (E-mail: v.krasnikov@chem.rug.nl)

Journal of Polymer Science: Part B: Polymer Physics, Vol. 41, 2665–2673 (2003)

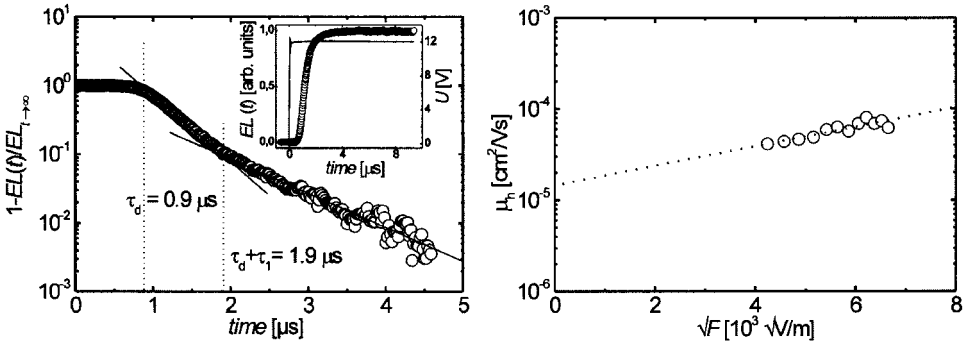

Figure 1. Left: transient EL for an ITO/PEDOT:PSS/MEH-OPV/Ca device. The insert shows the EL signal (○) and the applied voltage (—). Right: hole mobility versus square root of the electric field F obtained by transient EL measurements. The zero field mobility and the field activation factor were determined as $(1.5 \pm 1)\ 10^{-5}$ cm^2/Vs and $(2.5 \pm 1)\ 10^{-4}\ \sqrt{}$m/V, respectively.

hexoxy)benzene (MEH-OPV5) sandwiched between two metal contacts.

Another key issue, the influence of the morphology on the photovoltaic device performance itself, still needs to be tackled. Comparative studies on photovoltaic cells based on the donor–acceptor system are presented, revealing the influence of the morphology on the photovoltaic device characteristic. We explored single-layer, double-layer, and blended photovoltaic systems of vacuum-deposited donor MEH-OPV5 and acceptor buckminster fullerene (C_{60}) sandwiched between two metal contacts.

CHARGE TRANSPORT THROUGH SINGLE-LAYER MEH-OPV5 DEVICES

The photocurrent in a photovoltaic cell tends to saturate at higher light intensities because of space-charge effects,[9] which are more predominant in media of lower mobility. In a cell consisting of C_{60} and MEH-OPV5, for instance, the saturation of the photocurrent should be governed by the hole mobility in MEH-OPV5 as the electron mobility in C_{60} is rather high (up to 0.1 cm^2/Vs, depending on the crystallinity[10,11]). A frequently used technique to determine the charge-carrier mobility in strongly luminescent organic semiconductors is based on transient electroluminescence (EL).[12–14] The delay time between the rising edge of the voltage pulse and the appearance of the EL signal is, in general, determined by both the hole and the electron mobility. In materials with strongly different electron and hole mobilities, however, the transit of the slower carrier type can be neglected. In Figure 1, a typical EL signal in the pulsed regime is shown for a single-layer MEH-OPV5 cell. After an initial delay, the EL signal increases double exponentially. A detailed analysis of such EL transients was elaborated by Pinner et al.[14] In the frame of their model, the transit time for the holes is given by the delay time τ_d, after which the first recombination occurs, and τ_1, after which the charge distribution of the faster carrier species is built up. The increase in EL after $\tau_d + \tau_1$ is due to the establishment of the charge-carrier distribution of the slower electrons. In contrast to Pinner et al.,[14] however, the time constant of the second exponential increase was comparable to that of the first one, meaning that the electron distribution was established rather fast. This indicates that the electron mobility is lower but close to the hole mobility in MEH-OPV5. For MEH-PPV, similar observations have been reported.[15,16] As a consequence, the hole mobility determined with transient EL was slightly overestimated as the electron transit was not considered.

The hole mobility obtained from transient EL measurements as a function of the square root of the field is seen in Figure 1. At a field strength of $3\ 10^7$ V/m, a hole mobility in MEH-OPV5 of $6 \cdot 10^{-5}$ cm^2/Vs was measured, which is similar to the value given in ref. 17. Although the hole mobility in MEH-OPV5 was relatively high, it was far below the electron mobility in C_{60}. Thus, the saturation effects in the photocurrent at high light intensity were mainly determined by the MEH-OPV5 phase.

In highly disordered organic materials, the field and temperature dependency of the mobility

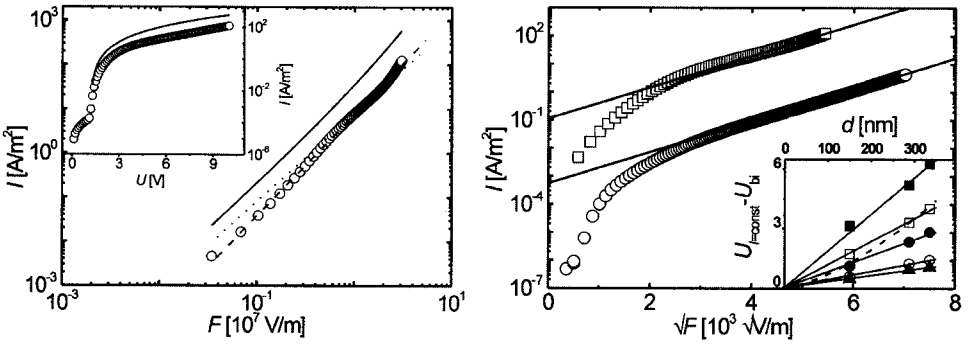

Figure 2. Left: IV characteristic of an ITO/PEDOT:PSS/MEH-OPV5/Al device (○). F is the electric field. The dotted line is a fit according to Child's law. A better fit is achieved with a power of 2.3 (dashed line). The continuous line is the SCLC calculated with the mobility parameters that were obtained from transient EL measurements. Right: IV characteristics of ITO/PEDOT:PSS/MEH-OPV5/Al and ITO/MEH-OPV5/Al devices. The insert shows the thickness dependency of bias at constant current for ITO/PEDOT:PSS/MEH-OPV5/Al devices. ■ (I = 25 A/m^2), □ (I = 10 A/m^2), ● (I = 5 A/m^2), ○ (I = 1 A/m^2), ▲ (I = 0.5 A/m^2). The dashed line is a fit for TFSCLC.

can be described with a correlated Gaussian disorder model.[18] Taking a typical intermolecular hopping distance of 1 nm, we obtained a disorder bandwidth around 0.07 ± 0.01 eV for MEH-OPV5. This is, in fact, nearly two times smaller than that of the corresponding polymers[15,19] as it is expected for more crystalline materials, resulting in an almost two times smaller field activation factor γ, namely, (2.5 ± 1) 10^{-4} (m/V)$^{1/2}$. In contrast, the zero field hole mobility of MEH-OPV5 was calculated as (1.5 ± 1) 10^{-5} cm^2/Vs, which is surprisingly high as compared with the values obtained for PPV-based polymers.[15,16,19]

Figure 2 presents the IV characteristic of a single-layer MEH-OPV5 device. In general, this kind of characteristic can be understood in terms of either space-charge or injection limitation. In the regime of space-charge-limited current (SCLC), the supply of injected carriers is sufficiently high so that bulk limitation dominates the current. The single-carrier trap-free space-charge-limited current (TFSCLC) is directly proportional to the charge-carrier mobility and is described by Child's law

$$j_{\mathrm{TFSCLC}} = 9/8\epsilon\mu\frac{U^2}{d^3}$$

where ϵ is the permittivity, μ is the charge-carrier mobility, U is the bias voltage, and d is the thickness of the film. It is a common approach to use SCLC conditions to determine the effective charge-carrier mobility.[17,20,21]

Recently, it was reported that the current through ITO/MEH-OPV5/Al diodes is SCLC, and in this context, IV characteristics were modeled over a wide voltage and current range.[17] According to our measurements, the IV characteristics indeed resemble SCLC in shape over a wide range in voltage and current (Fig. 2), although they differ in amplitude. This discrepancy is slightly relaxed because the mobility determined by transient measurements was overestimated. Obviously, however, additional independent justification like a proper thickness dependence[22] is required to confirm the presence of SCLC. In the insert of Figure 2, we show the required drive voltage at constant current in dependency of the thickness of the active layer. In the general case of a field-dependent mobility, the thickness dependence is described by d^{α}, where $1 < \alpha < 1.5$ holds for TFSCLC, whereas $\alpha = 1$ would be obtained in an injection-limited regime. Despite some random irreproducible variations in the current from sample to sample, the thickness dependence could not be approximated with a $d^{3/2}$ law, questioning the presence of SCLC and suggesting injection limitation.

Comparison of the IV characteristics of ITO/PEDOT:PSS/MEH-OPV5/Al and ITO/MEH-OPV5/Al devices depicted in Figure 2 is also in favor of injection limitation. The shapes of both IV curves are similar, but the amplitude is much smaller in the case of ITO/MEH-OPV5/Al. At higher bias, both curves exhibit a typical exponential behavior versus the square root of the field, resulting in a

field-activation factor of 1.29 10^{-3} $(m/V)^{1/2}$. On the basis of a drift-diffusion type of injection mechanism[8] suitable for low-mobility media and taking the field-activation factor of the mobility from transient EL measurements, a Schottky coefficient of $2.67 \cdot 10^{-5}$ eV $(m/V)^{1/2}$ was obtained. This is close to the theoretical value of $2.12 \cdot 10^{-5}$ eV $(m/V)^{1/2}$ found with a dielectric constant of 3.2.

The observed thickness dependence and the influence of the anode work function on the absolute value of current (but not on the shape) indicate that although the IV characteristics of the MEH-OPV5 cells show typical features of SCLC, the injection limitation is more likely. Our observation is in accordance with the results obtained by Shen et al.[23] The dependencies of injection-limited current and SCLC on the applied voltage can be very similar in shape for the reason that both currents are directly proportional to the charge-carrier mobility.

Charge transport through an organic semiconductor based on polymeric or oligomeric solids occurs via hopping among localized states. Consequently, the classical injection models formulated for inorganic materials have their limitations. Several injection models have been developed, considering the hopping nature of transport, strong charge localization, and both positional and energy disorder.[22–28] Our simulation of IV curves is based on a slightly modified phenomenological model proposed by Abkowitz et al.[29] According to this model, the charge injection and transport are described as thermally assisted tunneling in a one-dimensional uniformly spaced chain of hopping sites. Unlike Abkowitz et al.,[29] we allow only nearest-neighbor hops (multisite hopping is ignored). The thermally assisted tunneling of carriers from the metal to the organic material is, moreover, assumed to result only in the formation of a Boltzmann distribution at the first monolayer. The establishment of the charge-carrier distribution in the bulk occurs then by successive nearest-neighbor hopping events.

The model ignores any space-charge effects and cannot describe the transition to SCLC. As a consequence, the applicability of the model for devices with typical thickness and operational voltage is limited to barrier heights larger than 0.3 eV.

The rate at which a charge carrier occupying the state i moves to the empty state j is described in terms of the classical Marcus theory for the high-temperature limit[30]

$$R_{ij} \propto {}^1/\sqrt{T}\, e^{(E_i - E_j + \lambda)^2/4\lambda kT}$$

where E_i and E_j are the energies of the occupied site and the empty site, respectively; and λ is the reorganization energy. A typical value for the reorganization energy in disordered organic semiconductors of 0.3 eV was used. In general, the hopping rate from state i to j is the product of the Marcus rate for hopping, the probability to find a charge carrier at site i defined as p_i, and the probability to have the site j nonoccupied $(1 - p_j)$. To obtain the occupation probabilities of all sites, the principle of detailed balance was used. This principle requires the number of hops toward a certain site i to be equal to the number of hops leaving the same site. The spatial distribution of sites was set to be equidistant, with the interspacing of hopping sites equaling the molecule diameter. Detailed balance leads to the following set of equations:

$$R_{i-1,i}\, p_{i-1}(1 - p_i) + R_{i+1,i}\, p_{i+1}(1 - p_i) + p_i^{\text{bulk}} = R_{i,i-1} p_i(1 - p_{i-1}) + R_{i,i+1}\, p_i(1 - p_{i+1}) \quad \text{for } i = 2, \ldots, N-1$$

The occupation probabilities of sites 1 and N are related to the Boltzmann factor. p_i^{bulk} is the occupation probability of site i due to intrinsically generated charge carriers. As the occupation probability for site i in the injection-limited case is small, we approximated all probabilities to find an empty site to 1. The energies of the sites follow the potential $\Delta - qFx$, where Δ is given by the difference of the highest occupied molecular orbital level of the organic and the Fermi level of the metal, and F is the external electric field. Unlike Abkowitz et al.,[29] we included the image charge potential. Then, the current can be calculated by counting hopping events across any plane in the material.[29] However, to reduce the total number of fitting parameters and to calculate the absolute value of the current, we used the standard drift-diffusion expression for the current instead

$$J(x) = q\mu nF - kT\mu \frac{\partial n}{\partial x}$$

where $J(x)$ is the current density at position x, n is the calculated charge density obtained from detailed balance, and F is the field strength at x. The hole mobility (μ) was taken in the frame of the correlated Gaussian disorder model. The calcu-

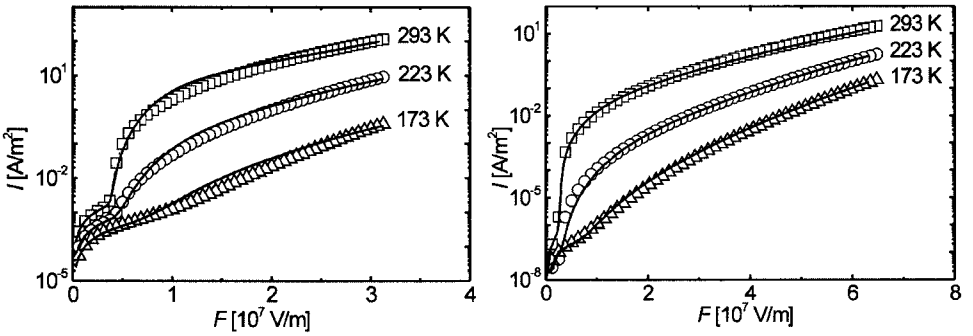

Figure 3. Left: current densities versus F of an ITO/PEDOT:PSS/MEH-OPV5/Al device for different temperatures (continuous lines). Right: current densities versus F of an ITO/MEH-OPV5/Al device for different temperatures (continuous lines). The scattered curves are fits according to the injection model.

lated currents (Fig. 3) agreed with the measured IV characteristics of the ITO/PEDOT:PSS/MEH-OPV5/Al and ITO/MEH-OPV5/Al devices. It is remarkable that not only the shape but also the absolute values of currents are simulated correctly, giving reasonable barrier heights of 0.39 and 0.53 eV at 293 K, respectively. Optimal fits were achieved with an energetic disorder bandwidth of around 0.06 eV and a zero-field hole mobility of 2.2 10^{-5} cm^2/Vs, which was close to the parameters obtained by transient EL measurements. However, the temperature dependency of the current could only be fitted with slightly decreasing barrier heights with decreasing temperature. Nevertheless, the change in barrier height was only 80 meV for the temperature range from 293 to 173 K. Such change in the calculated barrier height was likely the result of the energy disorder, which is not included in the model presented here. Moreover, dipole layers at the metal–organic interfaces[31] with temperature-dependent strength cannot be excluded.

DONOR–ACCEPTOR PHOTOVOLTAIC CELLS: ROLE OF MORPHOLOGY

Two basic donor–acceptor solid-state device structures for photovoltaic applications are in the main focus of interest—double-layer device structures with a single planar heterojunction interface[3,32,33] and systems of percolated donor–acceptor phases, that is, a network of heterojunctions throughout the entire film.[1,2,5] As a matter of course, the performance of the latter type of device is very sensitive to the morphology of the blend. Ideally (to ensure efficient exciton dissociation), an acceptor species should be within the exciton diffusion range from any donor species and vice versa. Moreover, both the donor and the acceptor phases should form a continuous network to allow bipolar charge transport. Because the exciton diffusion range is typically shorter than the light-absorption depth, the network of donor–acceptor heterojunctions should be more efficient in terms of the exciton dissociation than a conventional double-layer structure with a single planar donor–acceptor heterojunction. However, in the case of spatially distributed donor–acceptor heterojunctions, a possible partial discontinuity of the donor and/or acceptor phases may occur. Furthermore, the likely increased energy-level disorder in both phases may result in an increase of the charge-trap density and a reduction of the electron and/or hole mobility. Therefore, a degradation of the overall device performance could be expected. Obviously, a comparative study of both configurations requires the use of the same materials and identical preparation procedures. This requirement can be met with materials suitable for vacuum deposition.

In Table 1, we present the photovoltaic parameters of double-layered and codeposited cells on the basis of MEH-OPV5 as donor and C_{60} as acceptor material.[34] Surprisingly, our measurements revealed that the monochromatic power-conversion efficiency of the codeposited cell (1%) was about two times lower than that of the double-layer cell (>2%), although the exciton dissociation efficiency is expected to be higher in the first case because of the larger heterojunction interface. Similar observations have been reported for cells with indium tin oxide (ITO) as an anode material.[9] To unveil this unexpected result, one

Table 1. Main Cell Characteristics for Double-Layer ITO/PEDOT:PSS/MEH-OPV5/C_{60}/Al Cells, Codeposited ITO/PEDOT:PSS/MEH-OPV5 + C_{60}/Al Cells, Single-Layer MEH-OPV5, and C_{60} Cells.

	S (A/W)	FF	U_{oc} (V)	U_{soc} (V)	δ (eV)	N_i (10^{16} cm^{-3})	W_{0v} (nm)
Double layer	0.054	0.45	0.88	0.9 ± 0.1	0 ± 0.1	—	—
Blend	0.078	0.25	0.65	0.7 ± 0.1	0.2 ± 0.1	0.5 ± 0.1	210 ± 7
Single-layer MEH-OPV5	—	—	—	1.1 ± 0.1	−0.2 ± 0.1	—	—
Single-layer C_{60}	—	—	—	0.3 ± 0.2	0.6 ± 0.2	1.1 ± 0.4	110 ± 20

S is the photovoltaic sensitivity, *FF* is the fill factor, and U_{oc} is the open-circuit voltage measured at 1 mW/cm^2 light intensity at an illumination wavelength of 458 nm. U_{soc} is the saturated open-circuit voltage at the same wavelength, and δ is the effective dipole-layer shift. N_i and W_{0V} are the ionized state density and the depletion width at zero bias, respectively. The built-in potential U_{bi} was equal to U_{soc}

has to realize that the monochromatic power conversion efficiency is proportional to the photovoltaic sensitivity S as well as to the fill factor (FF) and the open-circuit voltage (U_{oc}):

$$\eta = S \cdot \mathrm{FF} \cdot U_{oc}$$

From Table 1, the slightly higher S of a codeposited device is compensated by its lower FF and U_{oc}, resulting in a decreased power-conversion efficiency as compared with the double-layer cell. To understand the difference of the obtained monochromatic power-conversion efficiencies in more detail, one has to trace back to the origin of the observed differences in S, FF, and U_{oc}.

The lower monochromatic power-conversion efficiency of cells on the basis of codeposited films is related, in part, to their lower fill factor. Intuitively, it seems reasonable that because of the intimate mixing of phases in a blend, the energetic disorder is increased, resulting in high trap densities and poorer transport properties and a lower FF. In a double-layer cell where intimate mixing is missing, the FF is higher because of the strongly reduced trap density.

The main advantage of percolated donor–acceptor photovoltaic systems is the strong increase of the heterojunction interface as compared with double-layer cells, which means a high level of photovoltaic sensitivity. Very efficient photovoltaic cells with this kind of percolated system have been produced.[5] Surprisingly, the S of a codeposited cell on the basis of MEH-OPV5 and C_{60} was not even twice as high as that of a double-layer cell.

To gain more insight into the relatively small increase in S, the surface morphologies of vacuum-deposited C_{60}, MEH-OPV5, and codeposited MEH-OPV5 + C_{60} on a solid substrate (mica) have been examined by atomic force microscopy (Fig. 4).[9] Thermal vacuum deposition of MEH-OPV5 resulted in the formation of large islands with an average height of about 30 nm, whereas the topography of C_{60} was smooth. The consecutively deposited cell appears to have an intermediate morphology between an interpenetrating blend and a truly planar double-layer film, exhibiting a finger-shaped interpenetrating pattern. Consequently, the area of the heterojunction interface was larger than that of an ideal double layer, approaching the area of a codeposited structure in terms of its availability for the dissociation of light-created excitons.

The power-conversion efficiency also depends on the open-circuit voltage. The saturated open-circuit voltage (U_{soc}) of a single-layer MEH-OPV5 cell approached 1.1 ± 0.1 V (Table 1), being close to the U_{soc} predicted by the metal/insulator/metal

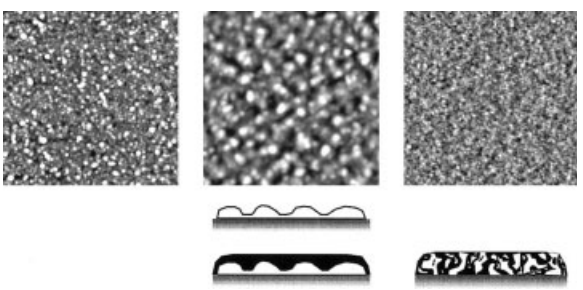

Figure 4. From left to right, the topography of C_{60} (20 nm maximum height), MEH-OPV5 (50 nm max height), and codeposited C_{60} + MEH-OPV5 (6 nm maximum height) on mica. Each graph is a scan of 2 × 2 μm. The sketches below indicate the device structure of a double-layer device and a codeposited device, respectively.

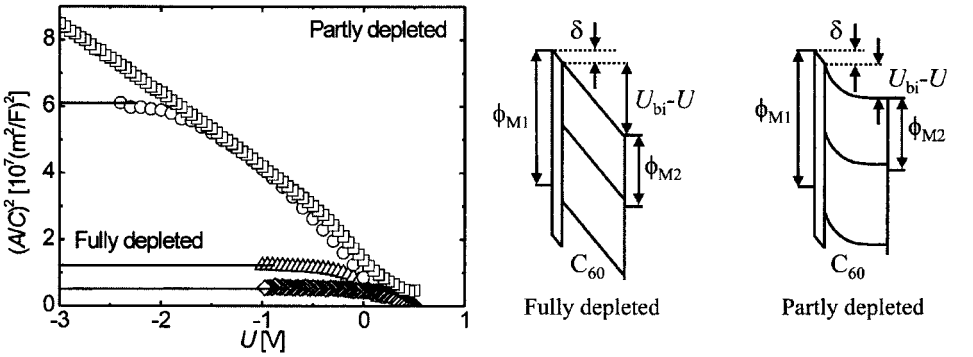

Figure 5. $(A/C)^2$ versus applied voltage for ITO/PEDOT:PSS/C_{60}/Al single-layer devices of 100 nm ◇, 130 nm △, 300 nm ○, and 500 nm □ thicknesses. The lines indicate the geometrical capacitance. The energy diagrams for fully and partly depleted conditions can be seen at the right.

(MIM) model ($U_{soc}^{MIM} \approx 0.9$ V), whereas the U_{soc} of a single-layer C_{60} cell was only 0.3 ± 0.2 V. Therefore, we attribute the decrease of U_{soc} from 0.9 ± 0.1 V in the double-layer cell to 0.7 ± 0.1 V in the codeposited cell to the influence of the C_{60} phase. Recent results of ultraviolet photoelectron spectroscopy revealed strong vacuum-level shifts at metal/C_{60} interfaces.[35] These shifts were assigned to either charge transfer toward C_{60} for low work-function metals (Ag) or hybridization in combination with partial charge transfer for high work-function metals (Au). As a consequence, the built-in potential in a single-layer C_{60} cell prepared under vacuum is strongly reduced. Similar effects were observed for MEH-OPV5.[31] The fact that a single-layer MEH-OPV5 device showed a U_{soc} predicted by the MIM model suggests, however, that the dipole-layer formation at the MEH-OPV/electrode interfaces is strongly suppressed. This conclusion is supported by the results obtained with double-layer devices, exhibiting a U_{soc} in accordance with the MIM model. Although we do not know the effect of the heterojunctions on the open-circuit voltage, it is reasonable to assume that dipole-layer shifts at the anode/MEH-OPV5 and the cathode/C_{60} interfaces do not occur. Accordingly, the main dipole-layer shift can be attributed to the C_{60} phase or, more specifically, to the anode/C_{60} interface with a total strength of about 0.6 ± 0.2 V.

CV measurements on single-layer C_{60} cells revealed a bias-independent geometrical capacitance at high frequencies (>1 kHz). At low frequencies (<100 Hz), a steep increase of capacitance in forward bias was observed. Several models including Schottky contact, *p-n* junction, charging of surface states, and so forth predict such bias-dependent capacitance with slow dynamics. In the low-frequency regime, a linear dependence of $1/C^2$ on bias unveils a depletion capacitance and provides simultaneously its built-in potential (U_{bi}), ionized state density (N_i), and the depletion width (W) (e.g., at zero bias).[8] For each cell, the obtained U_{bi} was close to the measured U_{soc}. Thus, considering the dipole-layer shifts, the MIM model predicted U_{soc} correctly. $1/C^2$ versus U for a 100-nm-thick single-layer C_{60} cell was linear only in a narrow range in forward bias, whereas in reverse bias the capacitance approached the geometrical capacitance. The film-thickness increase of C_{60} extended the depletion capacitance region toward reverse bias, corroborating a transition from a partly to a fully depleted cell (Fig. 5) and suggesting a one-side abrupt *p-n* heterojunction type of contact between C_{60} and one of the electrodes. Because a constant capacitance was observed over a wide range of bias and frequency for double-layer cells, the depletion layer was formed at the anode/C_{60} contact. We infer that the C_{60} layer was most likely *n*-doped with a rather low doping density of 10^{16} cm^{-3}. Although the origin of the doping is not known, Hayashi et al.[36] recently confirmed the formation of a Schottky barrier at the C_{60}/metal interface by imaging the band bending via the Kelvin probe technique. The doping of C_{60} was attributed to intrinsic impurities created during the preparation process of C_{60}.

Our interpretation of the cell characteristics is mainly based on the assumption that the interfacial dipole strength and the ionized state density are proportional to the corresponding material

density (i.e., volume fraction). Under this assumption, N_i is proportional to the density of C_{60}, and the dipole strength is proportional to the surface density of the organic medium at the metal–organic interface. Because we deposited C_{60} and MEH-OPV5 in a ration of 1:1, N_i of a codeposited structure should be half of N_i determined for the bare C_{60} film, and W_{0V} should be roughly two times longer, which was confirmed by CV measurements (Table 1). The interfacial MEH-OPV5 density in a blended cell is half of the interfacial MEH-OPV5 density of the bare MEH-OPV5 cell, resulting in a dipole-layer strength of −0.1 eV at the MEH-OPV5/metal interfaces. We considered the same for the C_{60}/metal interfaces in the blend, leading to a dipole-layer contribution of 0.3 eV. The predicted total dipole-layer strength in a blended cell is then 0.2 eV, and the U_{soc} (U_{bi}) should be 0.7 V, which is in agreement with the measured value (Table 1). Obviously, this simple dilution model relates device performance and morphology because it predicts very accurately the effective ionized state density N_i, the saturated open-circuit voltage U_{soc} (U_{bi}), and, consequently, the depletion width at zero bias W_{0V} for a codeposited photovoltaic cell.

CONCLUSIONS

We investigated the dark current diode characteristics of a single organic layer ITO/PEDOT:PSS/MEH-OPV5/Al diode. Experimental evidence was given that charge transport through these diodes is injection limited. With transient EL, the hole mobility of MEH-OPV5 was measured and subsequently used in IV simulations. A phenomenological injection model adequately described the IV characteristics over broad current and temperature ranges.

Moreover, we reported in great detail the influence of morphology on photovoltaic device performance. The difference in monochromatic power-conversion efficiency between double-layer and codeposited structures could be understood in terms of transport phenomena, interfacial effects, and morphology. The island formation of MEH-OPV5 and the potential of a device structure with interpenetrating fingers have been demonstrated. A Schottky contact at the interface between C_{60} and the high work-function metal was revealed. On the basis of a simple dilution model, the relation between the device performance and the morphology was rationalized.

The authors thank P. F. van Hutten for the many fruitful discussions. This research was financially supported by the Dutch Organization of Scientific Research (NWO-CW) and the Priority Program Materials.

REFERENCES AND NOTES

1. Halls, J. J. M.; Walsh, C. A.; Greenham, N. C.; Marseglia, E. A.; Friend, R. H.; Moratti, S. C.; Holms, A. B. Nature 1995, 376, 498–500.
2. Yu, G.; Gao, J.; Hummelen, J. C.; Wudl, F.; Heeger, A. J. Science 1995, 270, 1789–1791.
3. Granström, M.; Petritsch, K.; Arias, A. C.; Lux, A.; Anderson, M. R.; Friend, R. H. Nature 1998, 395, 257–260.
4. Roman, L. S.; Mammo, W.; Petterson, L. A. A.; Andersson, M. R.; Inganäs, O. Adv Mater (Weinheim, Ger) 1998, 10, 774–777.
5. Shaheen, S. E.; Brabec, C. J.; Sariciftci, N. S.; Padinger, F.; Fromherz, T.; Hummelen, J. C. Appl Phys Lett 2001, 78, 841–843.
6. Goetzberg, A.; Hebling, C. Solar Energy Mater Solar Cells 2000, 62, 1–19.
7. Sariciftci, N. S.; Smilowitz, L.; Heeger, A. J.; Wudl, F. Science 1992, 258, 1474.
8. Sze, S. M. Physics of Semiconductor Devices; Wiley: New York, 1981, pp 245–361.
9. Ouali, L.; Krasnikov, V. V.; Stalmach, U.; Hadziioannou, G. Adv Mater (Weinheim, Ger) 1999, 11, 1515–1518.
10. Jarret, C. P.; Pichler, K.; Newbould, R.; Friend, R. H. Synth Met 1996, 77, 35–38.
11. Rikitake, K.; Akiyama, T.; Takashima, W.; Kaneto, K. Synth Met 1997, 86, 2357–2358.
12. Braun, D.; Moses, D.; Zhang, C.; Heeger, A. J Appl Phys Lett 1992, 61, 3092–3094.
13. Blom, P. W. M.; Vissenberg, M. C. J. M. Phys Rev Lett 1998, 80, 3819–3822.
14. Pinner, D. J.; Friend, R. H.; Tessler, N. J Appl Phys 1999, 86, 5116–5130.
15. Bozano, L.; Carter, S. A.; Scott, J. C.; Malliaras, G. G.; Brock, P. J Appl Phys Lett 1999, 74, 1132–1134.
16. Scott, J. C.; Brock, P. J.; Salem, J. R.; Ramos, S.; Malliaras, G. G.; Carter, S. A.; Bozano, L. Synth Met 2000, 111–112, 289–293.
17. Jain, S. C.; Kapoor, A. K.; Geens, W.; Poortsmans, J.; Mertens, R. J Appl Phys 2002, 92, 3752–3754.
18. Novikov, S. V.; Dunlap, D. H.; Kenkre, V. M.; Parris, P. E.; Vannikov, A. V. Phys Rev Lett 1998, 81, 4472–4475.
19. Blom, P. W. M.; Vissenberg, M. C. J. M. Mater Sci Eng 2000, 27, 53–94.

20. Blom, P. W. M.; de Jong, M. J. M.; Vleggaar, J. J. M. Appl Phys Lett 1996, 68, 3308–3310.
21. Forero, S.; Nguyen, P. H.; Brütting, W.; Schwoerer, M. Chem Phys 1999, 1, 1769–1776.
22. Baldo, M. A.; Forrest, S. R. Physical Review B, Condensed Matter 2001, 64, 085201–085217.
23. Shen, Y.; Klein, M. W.; Jacobs, D. B.; Scott, J. C.; Malliaras, G. G. Phys Rev Lett 2001, 86, 3867–3870.
24. Wolf, U.; Arkhipov, V. I.; Bässler, H. Physical Review B, Condensed Matter 1998, 59, 7507–7513.
25. Arkhipov, V. I.; Emelianova, E. V.; Tak, Y. H.; Bässler, H. J Appl Phys 1998, 84, 848–856.
26. Arkhipov, V. I.; Wolf, U.; Bässler, H. Physical Review B, Condensed Matter 1999, 59, 7514–7520.
27. Barth, S.; Wolf, U.; Bässler, H.; Müller, P.; Riel, H.; Vestweber, H.; Seidler, P. F.; Rieß, W. Physical Review B, Condensed Matter 1999, 60, 8791–8797.
28. Scott, J. C.; Malliaras, G. G. Chem Phys Lett 1999, 299, 115–119.
29. Abkowitz, M. A.; Mizes, H. A.; Facci, J. S. Appl Phys Lett 1995, 66, 1288–1290.
30. Marcus, R. A.; Sutin, N. Biochim Biophys Acta 1985, 811, 265–322.
31. Veenstra, S. C.; Stalmach, U.; Krasnikov, V. V.; Hadziioannou, G.; Jonkman, H. T.; Heeres, A.; Sawatzky, G. A. Appl Phys Lett 2000, 76, 2253–2255.
32. Tang, C. W. Appl Phys Lett 1986, 48, 183–185.
33. Peumans, P.; Forrest, S. R. Appl Phys Lett 2001, 79, 126–128.
34. Melzer, C.; Krasnikov, V. V.; Hadziioannou, G. Appl Phys Lett, 2003, 82, 3101–3103.
35. Veenstra, S. C.; Heeres, A.; Hadziioannou, G.; Sawatzky, G. A.; Jonkman, H. T. Appl Phys A 2002, 75, 661–666.
36. Hayashi, N.; Ishii, H.; Ouchi, Y.; Seki, K. J Appl Phys 2002, 92, 3784–3793.